JOURNAL OF THERMOPHYSICS AND HEAT TRANSFER
Vol. 8, No. 1, Jan.–March 1994

Space Transportation System Launch Pad Summer Environmental Effects

R. A. Ahmad*
Thiokol Corporation, Brigham City, Utah 84302

The external tank (ET) of the space transportation system (STS) contains liquid oxygen and liquid hydrogen as oxidizer and fuel for the Space Shuttle main engines. This article describes a two-dimensional flow and thermal forced convection analysis to determine solar heat effects on the Space Shuttle launch components subsequent to the ET loading operation in extremely hot conditions. An existing computational fluid dynamics (CFD) code, parabolic hyperbolic or elliptical numerical integration code series (PHOENICS '81) was used in the study. The analysis was done for a two-dimensional slice between planes perpendicular to the longitudinal axis of the STS and passing through the lower portions of the redesigned solid rocket motors (RSRMs), the ET, and the orbiter wing. The results are presented as local and average values of surface temperatures and Nusselt numbers around the RSRMs and the ET. Solar heating effects increased surface temperatures of the RSRMs by 5–6.1°C. Comparisons were based on the local Nusselt number at the forward stagnation point and on the average Nusselt number around the West RSRM.

Nomenclature

D = diameter of RSRM, 12.2 ft (3.72 m) or ET, 28 ft (8.54 m)
Gr_D = Grashof number of free convection based on outer diameter of RSRM or ET, $g\beta(T_s - T_\infty)D^3/\nu^2$
g = acceleration due to gravity, ft/s² (m/s²)
h = convective heat transfer coefficient, Btu/h-ft²-°F (W/m²-°C)
IY, IZ = cell numbers in domain, Fig. 2
k = thermal conductivity of air, Btu/h-ft-°F (W/m-°C)
Nu_D = local Nusselt number based on outer diameter, hD/k
Pr = Prandtl number, 0.7
q''_{sol} = solar heat flux, Btu/h-ft² (W/m²), Fig. 3
Re_D = Reynolds number of forced convection, $U_\infty D/\nu$
T = temperature, °F (°C)
t = half the thickness of adjacent air cell to a surface, in. (mm)
U_∞ = freestream wind velocity, ft/s (m/s)
Y, Z = Cartesian coordinates, Figs. 2 and 4
β = coefficient of volumetric expansion of air, $1/T_\infty$, °R⁻¹ (K⁻¹)
ε = dissipation rate of turbulence kinetic energy per unit mass, (ft²/s²)/s (m²/s²)/s
θ = angular direction, deg (Figs. 2 and 3)
κ = turbulence kinetic energy per unit mass, ft²/s² (m²/s²)
μ = dynamic viscosity, lbm/ft-s (kg/m-s)
ν = kinematic viscosity of air, μ/ρ, 0.6482 ft²/h (6.0221×10^{-2} m²/h)
ρ = air density, lbm/ft³ (kg/m³)

Subscripts
c = cell adjacent to a surface
D = based on diameter
fsp = forward stagnation point on the west RSRM, $\theta \simeq 150$ deg
i = inside RSRM cavity or ET fuel tank
l = laminar
m = arithmetic mean, measured
s = surface
sol = solar
t = turbulent
∞ = freestream conditions

Superscript
$-$ = average

Presented as Paper 92-3850 at the AIAA/SAE/ASME/ASEE 28th Joint Propulsion Conference, Nashville, TN, July 6–8, 1992; received July 15, 1992; revision received Feb. 19, 1993; accepted for publication Feb. 19, 1993.

*Scientist and Member of the Technical Staff, Engineering Analysis Department, Space Operations, M/S L63, P.O. Box 707. Senior Member AIAA.

Introduction

THE external tank (ET) of the space transportation system (STS) contains 146,000 gal (552.61 m³) of liquid oxygen (LOX) and 393,000 gal (1487.51 m³) of liquid hydrogen (LH_2) as oxidizer and fuel for the Space Shuttle main engines (SSMEs). The thermal protection system (TPS) of the ET is required to maintain the ET and the redesigned solid rocket motors (RSRMs) and their propellants within design temperature limits prior to launch. The TPS for the ET prior to launch is designed to 1) ensure propellant quality; 2) control LOX and LH_2 boil-off rates; 3) maintain LOX and LH_2 oxidizer and fuel loading accuracies; and 4) minimize liquid propellant stratification.

For solid propellant rocket motors, propellant mean bulk temperature (PMBT) is a slowly varying function of wind velocity, ambient temperature, solar heat flux, time, and other factors. Common practice[1] in developing and testing rocket motors is to condition the motor for many hours at a particular temperature before firing to ensure the propellant grain is uniformly at the desired temperature. The higher the PMBT, the higher the burn rate will be, the higher the thrust, the higher the specific impulse, and the shorter the burn time. These in turn affect the selection of flight trajectory. Knowledge of the increase in surface temperature would enable calculating the increase in burn rate[1] due to the increase in PMBT.

To determine the solar heat effect in extremely hot conditions, the STS' adjoining flow/thermal field must be known with sufficient accuracy so that Nusselt number values can be determined at the STS component surfaces. Previous pertinent thermal modeling studies of the STS are given chronologically in Refs. 2–18. Most of these concerned cold ambient

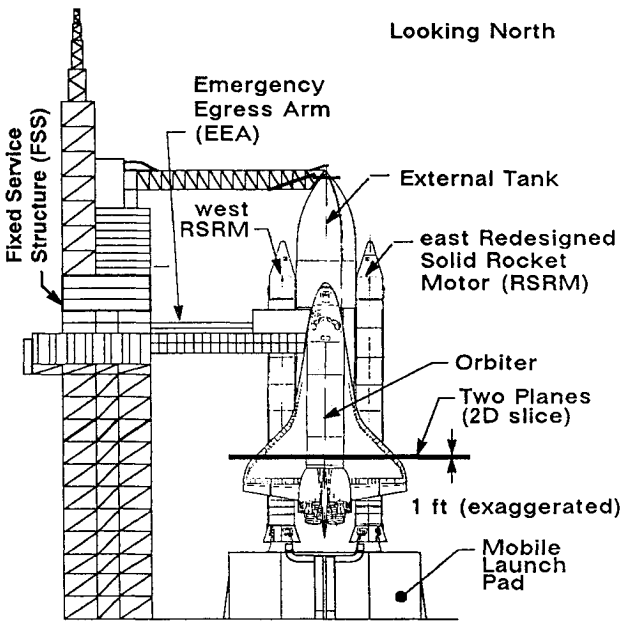

Fig. 1 STS on launch pad.

conditions of the STS on the launch pad. The purpose of this study was to obtain a more accurate assessment of the heating effect by using more accurate values of the Nusselt numbers. Values in the literature are generally inappropriate for the low-wind/multiple, large-cylinder configuration typified by the STS on the launch pad. The needed Nusselt number values were obtained from a calculation of the flow/thermal field using STS geometry and parabolic hyperbolic or elliptical numerical integration code series (PHOENICS '81) flow/thermal code.[19,20] PHOENICS '81 is a broadly accepted, tested, multidimensional, general-purpose computational fluid dynamics (CFD) computer code for the analysis of fluid flow, heat transfer, and chemical reaction problems.

The flow/thermal field was calculated in a plane parallel to and through a slice between two planes perpendicular to the STS longitudinal axis, and passing through the lower portions of the RSRMs, ET, and orbiter wing (Fig. 1).

Results from this study and other related studies[11,13,14,16] were first used to provide accurate boundary conditions for a three-dimensional global thermal model (GTM)[17] using the systems improved numerical differencing analyzer (SINDA) thermal conduction code,[21] which had been developed for use during the solid rocket motor (SRM) redesign. Results also provided accurate coefficients for use in designing the heaters for RSRM case and igniter joints, determinating the required temperature conditioning of the region between the RSRM aft skirt and nozzle, and in predicting the RSRM PMBT. In this study, the solution provided the necessary flow/thermal information whereby the thermal field was solved by using a forced convection heat transfer mode. Local and average values of the surface temperatures and Nusselt number around the RSRMs and ET were calculated.

Previous Work

Reference 2 describes an experimental study to determine the forced convection heat transfer coefficient at the surface of a LOX-filled tank 18 in. (0.46 m) in diameter, 22 ft (6.71 m) high, and having a 0.094-in.- (2.39-mm-) thick wall of 304 stainless steel. The average convective heat transfer coefficient was correlated in the form

$$\bar{h} = \frac{0.355(T_\infty/100 + 1.6)}{(D_0)^{0.195}} \left(\frac{U_\infty}{T_\infty/100 - 0.712}\right)^{0.805} \quad (1)$$

where D_0 is the outside cylinder diameter, taken as 1.5 ft (0.46 m) for any cylinder larger than 1.5 ft (0.46 m), U_∞ (kt), and T_∞ (°R).

In Ref. 4, the emphasis was on evaluating the temperatures of the lower-right SRM segment during a period of several hours before launch and after completion of the ET tanking operation. In that study, the heat transfer coefficient around the SRM was selected to be in the range of 0.5–4 Btu/h-ft²-°F (2.84–22.71 W/m²-°C) for wind speeds of 0–20 mph (0–8.94 m/s).

A three-dimensional model was developed by Mahaffey and Keeton[5] using PHOENICS to calculate local air temperatures around the STS. It deals with buoyancy effects imposed on forced convection. The number of cells used in this three-dimensional model was 33 by 25 by 30, a total of 24,750 cells.

Singhal et al.[6] had determined the feasibility of using hot-gas jets to prevent prelaunch ice formation on the ET which could break up during launch and damage ceramic tiles on the underside of the orbiter. In that study, the PHOENICS code with a Cartesian coordinate system adequately modeled the three-dimensional jet/ambient thermal environment. The number of cells used in this three-dimensional model was 12 by 16 by 22, a total of 4224 cells.

Mahaffey et al.[7] in a later study developed a model using PHOENICS for the region between the SRMs and ET. A finer grid than the above model[5] was used to resolve the thermal boundary layer. Results of the first model were used in the second model as boundary conditions at the desired locations. In both models,[5,7] heat transfer results and surface temperatures were not reported.

The latest version of the thermal interfaces design data book (TIDDB)[12] provided the surface temperatures at the lower portions of the east and west SRMs, which correspond to the slice considered in this study, as 110°F (43.33°C) and 105°F (40.56°C) at 1300 h over 3 days, respectively. This study used the SINDA[21] and thermal radiation analysis system (TRASYS)[22] computer codes, along with wind-tunnel measurements of local wind velocities around the RSRMs and ET. The local measured wind velocities were used to calculate the local Reynolds number around the RSRMs and ET. These values[9] were substituted in a correlation for turbulent flow on a flat plate to calculate the local forced convection heat transfer coefficients. For north wind, the average heat transfer coefficient around the SRM and ET were calculated to be 2.93 Btu/h-ft²-°F (16.64 W/m²-°C) and 2.53 Btu/h-ft²-°F (14.37 W/m²-°C), respectively.

Reference 15 described an experimental investigation of crossflow of air around a tandem three-cylinder model in a wind tunnel. The center and aft cylinders were cooled and heated, respectively, to promote sustained heat transfer with the surrounding airflow during tests. This setup resembles the STS prelaunch configuration; however, the forward cylinder was not heated. This simulation represents a situation that would promote thrust imbalance. It is of little value to STS modeling because of a requirement to have both boosters at similar propellant temperatures so that any differential thrust falls within a thrust envelope that can be accounted for. Apparently, the intent was to find the cooling effect of the center cylinder on aft cylinder.

Reference 23 provided peak prelaunch surface temperatures measured on the east and west SRMs/RSRMs during prior STS launches. Table 1 shows the most recent measured peak surface temperatures ($T_{s,m}$) on the RSRMs during the 25 most recent STS launches. Resistance temperature detectors (RTDs) were placed to measure against cold surface temperatures at 40 locations per RSRM.

In all previous studies, Nusselt number was either of no interest,[3] estimated,[4,9,12] not reported,[5–7] or reported.[2,10,11,13–16] A literature review reveals that several important aspects of forced convection flows are still unknown. Therefore, the following conclusions may be drawn:

Table 1 Peak prelaunch surface temperatures measured on the east and west RSRMs

No.	Launch	Date	Time, EST[a]	T_{∞},[23] °F (°C)	East RSRM $T_{s,m}$,[23] °F (°C)	West RSRM $T_{s,m}$,[23] °F (°C)
1	STS-26	09-29-88	11:37	84 (28.9)	88 (31.1)	83 (28.3)
2	STS-27	12-02-88	09:30	56 (13.3)	72 (22.2)	74 (23.3)
3	STS-29	03-13-89	09:57	65 (18.3)	75 (23.9)	74 (23.3)
4	STS-30	05-04-89	14:46	78 (25.6)	93 (33.9)	86 (30.0)
5	STS-28	08-08-89	08:37	83 (28.3)	88 (31.1)	90 (32.2)
6	STS-34	10-18-89	12:53	85 (29.4)	96 (35.6)	88 (31.1)
7	STS-33	11-22-89	19:23	72 (22.2)	85 (29.4)	75 (23.9)
8	STS-32	01-09-90	07:35	58 (14.4)	69 (20.6)	69 (20.6)
9	STS-36	02-28-90	02:50	69 (20.6)	78 (25.6)	80 (26.7)
10	STS-31	04-24-90	08:33	71 (21.7)	75 (23.9)	77 (25.0)
11	STS-41	10-06-90	07:47	80 (26.7)	86 (30.0)	86 (30.0)
12	STS-38	11-15-90	18:48	75 (23.9)	91 (32.8)	90 (32.2)
13	STS-35	12-02-90	01:49	72 (22.2)	75 (23.9)	74 (23.3)
14	STS-37	04-05-91	09:22	73 (22.8)	83 (28.3)	77 (25.0)
15	STS-39	04-28-91	07:33	75 (23.9)	85 (29.4)	85 (29.4)
16	STS-40	06-05-91	09:25	79 (26.1)	85 (29.4)	86 (30.0)
17	STS-43	08-02-91	11:02	82 (27.8)	94 (34.4)	91 (32.8)
18	STS-48	09-12-91	19:11	81 (27.2)	99 (37.2)	93 (33.9)
19	STS-44	11-24-91	18:44	64 (17.8)	86 (30.0)	77 (25.0)
20	STS-42	01-22-92	00:00	63 (17.2)	72 (22.2)	62 (16.7)
21	STS-45	03-24-92	00:00	66 (18.9)	62 (16.7)	62 (16.7)
22	STS-49	05-07-92	00:00	68 (20.0)	75 (23.9)	74 (23.3)
23	STS-50	06-25-92	00:00	84 (28.9)	91 (32.8)	85 (29.4)
24	STS-46	07-31-92	09:57	84 (28.0)	94 (34.4)	86 (30.0)
25	STS-47	09-12-92	10:23	82 (27.8)	92 (33.3)	90 (32.2)

[a]EST: Eastern Standard Time, $°C = \frac{5}{9}[T_{\infty}(°F) - 32]$.

1) There is a general lack of experimental and theoretical work analyzing multiple large cylinders in series as typified by the two RSRMs and the ET.

2) Results of heat exchanger studies for flow around banks of cylinders could not be applied directly since these studies were based on transverse and longitudinal pitch. There is no transverse pitch in STS geometry for the flow direction considered in this study. In addition, the orbiter wing further complicates the geometry.

3) The condition of dynamic similarity cannot be fully satisfied. Under conditions of low wind velocities and large cylinder diameters the problem is not of pure forced convection, but rather where forced and free convection coexist, and thus must be treated simultaneously. For example, two extreme cases might be a) free convection with a large cylinder and low velocity, and b) forced convection with a small cylinder and high velocity. Thus, equivalent Reynolds numbers which constitute dynamic similarity might be misleading.

Present Study

In this study, the PHOENICS '81 code was used to determine a more exact flowfield of the STS launch pad environment and, consequently, more exact Nusselt number values. These permitted a more precise calculation of the solar heating effect in terms of the RSRM and ET local surface temperatures.

A comparison of the Reynolds number (Re_D) to the Grashof number (Gr_D) around the RSRMs and ET would be useful. Air properties are taken to be constant and evaluated at the ambient temperature of 99°F (37.22°C). Reynolds number is calculated to be 6.78×10^5 and 1.56×10^6 for the RSRM and ET, respectively. Temperature differences between the surfaces of the RSRM and ET and ambient were assumed, respectively, as 10°F (5.56°C) and 30°F (16.67°C) (not known, a priori). Grashof number is calculated to be 3.23×10^{10} and 1.17×10^{12} for the RSRM and ET, respectively.

Following the study of mixed convection from vertical cylinders by Oosthuizen and Taralis[24] in defining the buoyancy parameter as $\kappa' \equiv Gr_D/(Re_D)^2$, and using the above calculated values of Re_D and Gr_D yield values of 0.07 and 0.48 for the RSRM and ET, respectively. Using a lower value than 10 ft/s (3.05 m/s) for U_{∞} would violate this criterion[24] and require a third spatial dimension to account for free convection. Specifically, for U_{∞} equal to 7 ft/s (2.13 m/s) a value of 1 would result for κ' (based on ET). In this case both free and forced convection coexist and therefore must be treated simultaneously. Furthermore, in an experimental study using air, Collis and Williams[25] recommended that the free convection contribution in mixed convection over a horizontal cylinder be considered negligible when $Re_D > (Gr_D)^{1/3}$. Using values calculated for Re_D and Gr_D, this requirement has been met. Based on these two methods, the assumption of forced convection is sound.

The governing equations within PHOENICS '81, the numerical model, and the boundary conditions used in this study are discussed in this section.

Governing Equations

PHOENICS '81 uses a fully conserved and implicit formulation to solve the transport equations. Conservation of phase-mass, momentum, energy, chemical species, and turbulence kinetic energy and its dissipation rate are expressed in PHOENICS '81 by the general partial differential equation[19,20]

$$\frac{\partial}{\partial t}(r_i\rho_i\phi_i) + \nabla\cdot(r_i\rho_i v_i\phi_i - r_i\Gamma_{\phi i}\nabla\phi_i) = r_i S_{\phi i} \qquad (2)$$

where ϕ_i is the ith component of the conserved property ϕ; r_i and ρ_i are the volume fraction and density of ϕ_i; and $\partial/\partial t(r_i\rho_i\phi_i)$, $\nabla\cdot(r_i\rho_i v_i\phi_i)$, and $\nabla\cdot(r_i\Gamma_{\phi i}\nabla\phi_i)$ denote its transience, convection, and diffusion, respectively. The term $\Gamma_{\phi i}$ is the exchange coefficient for ϕ_i, and $S_{\phi i}$ defines its source(s). In laminar flows, the exchange coefficient Γ_{ϕ} is μ for momentum, μ/Pr for energy, and μ/Sc for chemical species (Sc is Schmidt number).

The partial differential equation for each of the conserved quantities is converted to a finite difference form using a staggered grid and hybrid-differencing[26] scheme. Integration of the partial differential equation led to a set of finite volume

equations, one equation for each conserved quantity, which were solved iteratively.

PHOENICS '81 has the flexibility to represent solid obstructions in the flowfield by the porosity concept.[19,20] Porosities are used to modify Cartesian or polar grid cells. There are four porosities for each cell: the cell porosity represents the proportion of cell volume available for occupancy by the flow; and the other three represent three faces of the cell which are available for occupancy by the flow.

Numerical Model

The primary task in this study was the determination and analysis of the two-dimensional flow/thermal field generated by a northwest wind (Fig. 1). This study is an extension of the study described in Ref. 13. Additional details of this study can be found in Refs. 11 and 18. Generation of this field assumed the flow to be steady, turbulent, and elliptic.

The inner temperatures of the RSRMs and ET, along with solar heat flux and the ambient temperature, served as thermal drivers. With heat conduction considered through the walls of the RSRMs and ET, in addition to the heat convection at their outer surface, the flow/thermal analyses were truly conjugate.

The local surface temperature of either the RSRM or ET was calculated from an energy balance between the air cell adjacent to a surface and the surface. There are three heat transfer rates. On a unit area basis they are 1) conduction through N layers of a composite wall ($q''_{K,i}$); 2) conduction through a thin air cell ($q''_{K,c}$); and 3) solar heat flux to the surface [$\alpha' q''_{sol}(\theta)$]. Substituting for the individual heat transfer terms and solving for T_s yield

$$T_s(\theta) = \frac{(k/t)T_c(\theta) + GT_i + \alpha' q''_{sol}(\theta)}{(k/t) + G} \tag{3a}$$

where the thermal conductance

$$G = \sum_{j=1}^{N} (K/L)_j \tag{3b}$$

The layer thickness L and thermal conductivity K for each of the components layers in the RSRMs and ET are specified as in Ref. 16. Solar absorptivity α' for both the RSRMs and ET is given as 0.5.[12]

In this model, inlet values for the kinetic energy of turbulence (κ_{in}) and its dissipation rate (ε_{in}) must be specified as boundary conditions. The κ-ε turbulence model assumes the fluctuations from the average velocity in three directions to be equal ($u' = v' = w'$). Therefore, the inlet kinetic energy of turbulence per unit mass was calculated as

$$\kappa_{in} = 3(u')^2/2 \tag{4a}$$

The level of turbulence intensity ($I_t = u'/U_\infty$) approaching STS was assumed to be 2.5%. The dissipation rate at inlet per unit mass was calculated as

$$\varepsilon_{in} = c_\mu(\kappa_{in})^{3/2}/L_t \tag{4b}$$

where the constant c_μ is taken as 0.09,[27] and L_t is the characteristic length scale of turbulence and was assumed as 0.01 times the diameter of the ET. In turbulent flow, the exchange coefficient Γ_ϕ in Eq. (2) is replaced by an "effective" exchange coefficient. In particular, μ is replaced by the effective viscosity μ_{eff} which is calculated as

$$\mu_{eff} = \mu_l + \mu_t \tag{4c}$$

In the κ-ε turbulence model, the local turbulent or eddy viscosity (μ_t) is calculated from the local scaler values of κ and ε as

$$\mu_t = c_\mu \rho \kappa^2/\varepsilon \tag{4d}$$

PHOENICS '81 has special built-in wall functions[19,20] for turbulent flows. The Reynolds number is first evaluated based on the tangential component of air velocity at a perpendicular distance from the surface. If this is less than 132.25, the wall shear stress is evaluated from the assumption of a linear velocity profile between the calculated near-wall value and the prescribed wall value, and the laminar viscosity is used. If the Reynolds number turns out to be greater than 132.25, the presumed velocity variation is assumed to be logarithmic, and the corresponding wall shear stress is evaluated. This corresponds to the commonly used "log-law" wall function.

Figure 2 shows the two-dimensional solution domain used in the determination of the flow/thermal field. The domain had a highly nonuniform grid to permit a better resolution in the areas of interest. The two-dimensional domain [146 by 88 ft (44.5 by 26.8 m)] was divided into 138 by 75 cells (a total of 10,350 cells) in the Y and Z directions, respectively.

A Cartesian coordinate system with stepped walls was used in this study because of the complex geometry. Although body-fitted coordinates (BFC) were available, they were not widely used at the time this study was initiated. The choice of a Cartesian system also allowed for ease of setup and computational economy, although the BFC coordinates may have

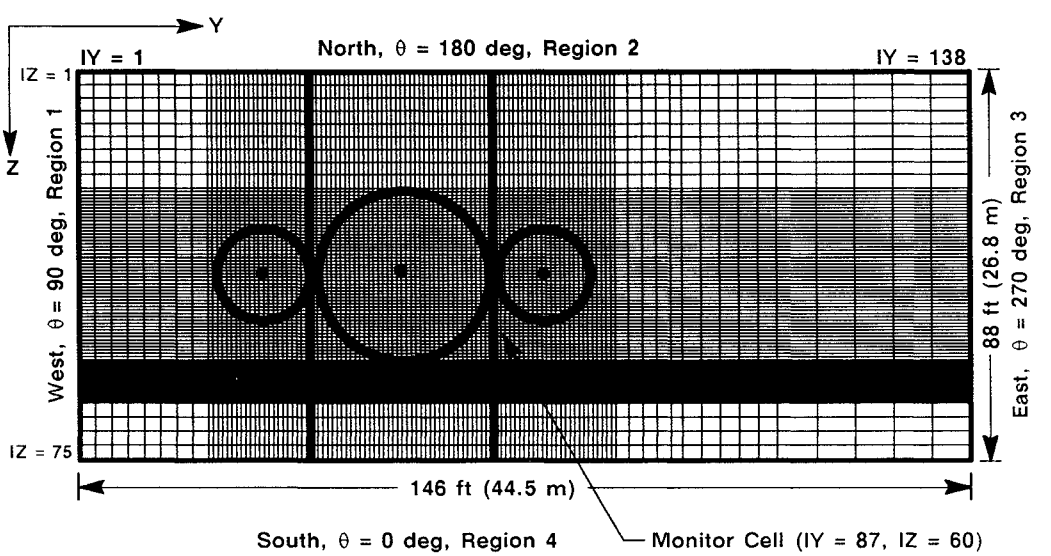

Fig. 2 Two-dimensional computational grid of STS components.

provided greater accuracy in the heat transfer results. In a supporting analysis,[28] the method of partial porosity was used to represent the RSRM surface more accurately. It was shown that the quality of the solution was not improved.

The final size of the domain had been determined in an earlier study,[29] where starting from a small grid the number of grid points was gradually increased until grid-independent results were achieved. Several grid sizes were examined before choosing the final grid of 138 by 75 cells.

Convergence of a PHOENICS '81 solution is generally achieved as follows:

1) Convergence is achieved by calculating the domain sum of the absolute value of the volumetric imbalances of each cell divided by a reference value of a residual. This ratio is reported in the PHOENICS '81 output after a number of sweeps have been run. If it diminishes systematically with sweep number, then the solution is converging.

2) Monitoring a cell within a region of the flow that is of particular interest achieves convergence, either from an engineering standpoint or because convergence difficulties are expected within that region. A monitor cell allows the user to observe the progress of the solution.

3) Furthermore, iterative procedure of repeated sweeps is terminated if, at the end of any sweep, the sum of the absolute volumetric continuity errors for all cells in the flow domain is less than the "level of convergence" set by the user. The level of convergence set in this study varied between 10^{-3}–10^{-4} for all variables.

Boundary Conditions

The boundary conditions used in this analysis are as follows:

1) Ambient temperature[30] was assumed to be 99°F (37.22°C).

2) Angular solar heat fluxes[8] for the RSRMs (given in Fig. 3) were used. The heat flux for the west RSRM was used for the ET.

3) The approaching airflow was assumed to be at a speed of 10 ft/s (3.05 m/s). Its direction[13] was 30-deg south of north (Fig. 4).

4) The air temperature in the RSRM bore was assumed to be that of the PMBT at 82°F (27.78°C). At 99°F (37.22°C), this was the hottest PMBT ever experienced.[3]

5) The temperature at the inner boundary of the ET for the fuel tank was assumed to be that at which hydrogen liquefies[31] [−423°F (−252.78°C)].

6) Thermal radiation exchange was assumed to be negligible. A typical maximum of 2°F (1.11°C) difference in temperature results when included.

7) Mass flux, velocity, enthalpy, and κ and its ε were applied as input boundary conditions along the domain's inlet, regions 1 and 2 (Fig. 2).

8) Flow was allowed to enter or exit at the outlet regions 3 and 4 (Fig. 2), depending on the local calculated difference between the near-boundary grid pressure and ambient pressure.

9) The surface of the orbiter was assumed to be adiabatic.

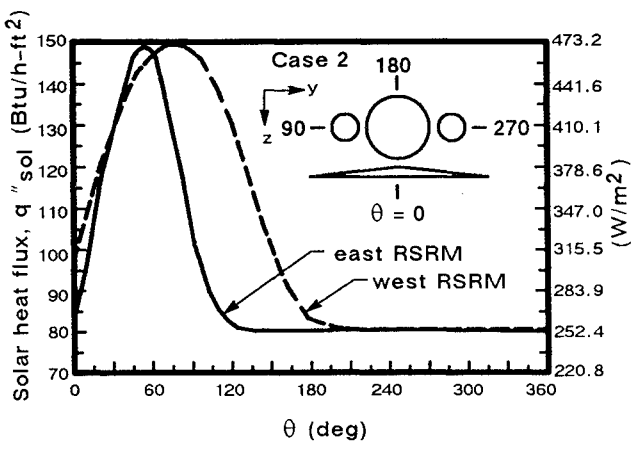

Fig. 3 Solar heat flux at 1300 hr in June at launch site.

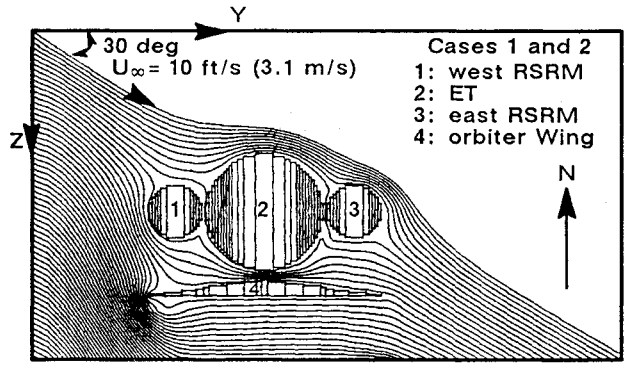

Fig. 4 Two-dimensional streamlines around STS components.

Results and Discussion

The numerical model and the imposed boundary conditions were used to make two calculations of the flow/thermal field surrounding the STS components. The first of these was conducted without solar heating; the second considered solar heating.

Because of the concern with flow convergence within the wake of the ET for the previously assumed west wind, a monitor cell was chosen to lie on the leeward side of the ET. Identified by the cell number $IY = 87$ and $IZ = 60$, this cell is shown in Fig. 2. Calculations of flow/thermal variables within the entire domain were made. Results of some of these calculations, such as the streamlines around the STS components as shown in Fig. 4, are common to both cases. These streamlines are shown to adjust to the presence of the STS components. Vortices have not appeared because of the low velocity and easy conformance of the airflow to the surface contours of the STS components. This flowfield compares very well with the results of a similar earlier study.[10] As expected, the flowfield is distinctly different than a typical flowfield around a single cylinder.

The local level of turbulence viscosity in a cell predicted by the two-equation (κ-ε) turbulence model can be calculated from the local values of κ and ε at that cell by Eq. (4d). Figure 5 shows the level of the turbulence viscosity (μ_t) and the local scale of turbulence, L_t, in the wake region and extending to the exit region (region 3 of Fig. 2) for $IZ = 60$ and $IY = 120$ to 138.

The local Nusselt number $Nu_D(\theta)$ around the RSRM or ET was calculated as

$$Nu_D(\theta) = h(\theta)\frac{D}{k} = \frac{-k\left[\left(\frac{\partial T}{\partial n}\right)_s\right]}{T_s(\theta) - T_\infty}\left(\frac{D}{k}\right) \qquad (5)$$

where $(\partial T/\partial n)_s$ is air temperature gradient, measured at the surface in a direction normal to the surface and calculated linearly between the surface temperature and the temperature of the adjacent cell to a surface.

The average values of the Nusselt number was obtained by integrating the local values around the RSRMs and ET.

Case 1: Without Solar Heat Flux

In this case, solar heat flux was not considered. Maximum temperature variation in the angular direction for both RSRMs is 1°F (0.56°C). Average circumferential surface temperatures of both RSRMs were calculated to be 92°F (33.3°C). The maximum temperature variation in angular direction for the ET is also 1°F (0.56°C). The average circumferential surface temperature of the ET was calculated to be 54.16°F (12.22°C).

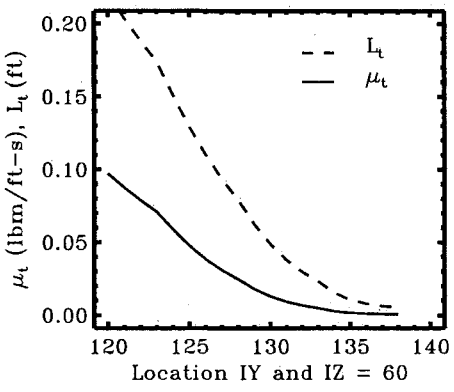

Fig. 5 Level of local turbulence viscosity and local scale of turbulence. All are in the wake region of the cylinders at selected location of Fig. 2.

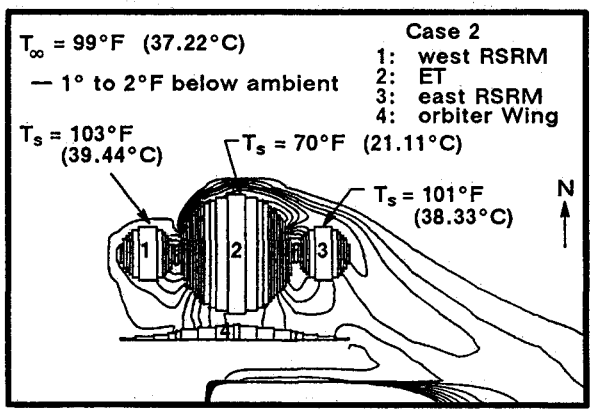

Fig. 6 Isotherms around STS components.

Case 2: With Solar Heat Flux

In this case, solar heat flux for the RSRMs and ET was included. It is given for a clear summer day at 1300 h (June 21)[8] (Fig. 3). The local surface temperature was then calculated from Eq. (3). The results for this case are also given in Figs. 4–8 and are summarized as follows:

1) Figure 6 shows the computed isotherms in the vicinity of the STS components. Local surface temperatures around the RSRMs and ET are shown in Figs. 7a and 7b, respectively. A maximum circumferential variation was found to be 7°F (3.89°C) and 11°F (6.11°C) around the RSRMs and ET, respectively. Average surface temperatures of the west RSRM, east RSRM, and ET were calculated to be 103°F (39.44°C), 101°F (38.33°C), and 70°F (21.11°C), respectively. The solar heat flux altered surface temperature profiles for three surfaces. Furthermore, solar heat flux results in an additional temperature rise of 11°F (6.11°C), 9°F (5°C), and 16°F (8.89°C) in the average surface temperatures of the RSRMs and ET, when compared with case 1 results. These surface temperatures are higher than ambient temperature by 4°F (2.22°C) and 2°F (1.11°C) for the west and east RSRMs, respectively. The surface temperature of the ET is 29°F (16.11°C) lower than ambient temperature.

The measured peak temperatures[23] given in Table 1 are independent of this study. They were fitted with straight lines as functions of the ambient temperature in the range of 56°F (13.33°C) $\leq T_\infty \leq$ 85°F (29.44°C):

east RSRMs

$$T_s(°F) = 15.51 + 0.92\ T_\infty(°F) \qquad (6a)$$

west RSRMs

$$T_s(°F) = 19.89 + 0.82\ T_\infty(°F) \qquad (6b)$$

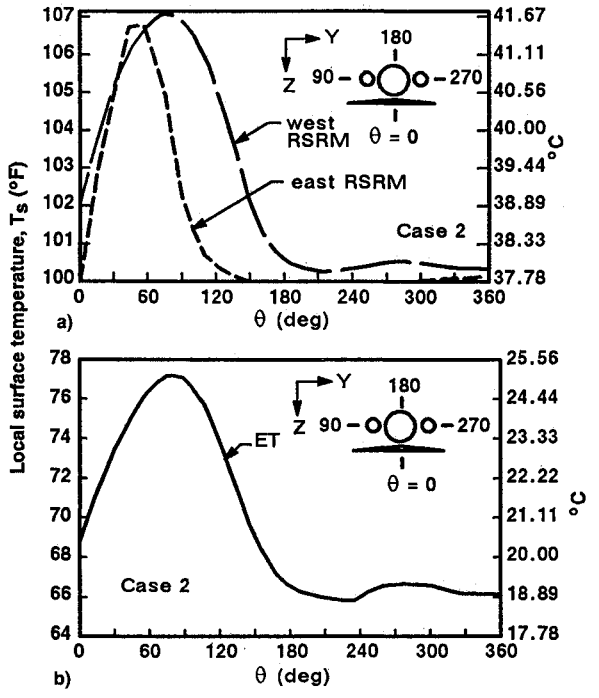

Fig. 7 Local surface temperature around a) RSRMs and b) ET of STS on launch pad.

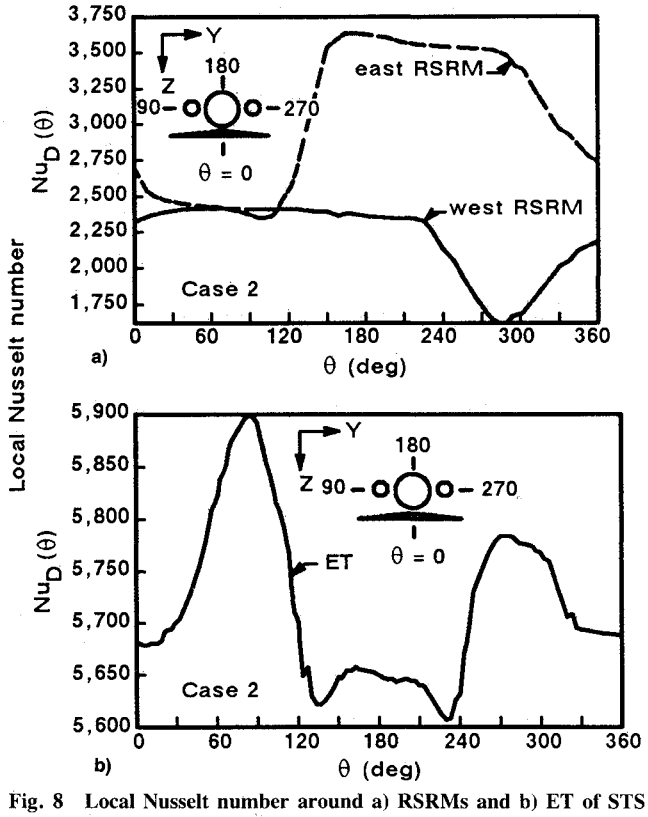

Fig. 8 Local Nusselt number around a) RSRMs and b) ET of STS on launch pad (with solar heat flux).

These correlations are shown in Fig. 9. Using the above derived correlations, expected surface temperatures on the east and west RSRMs would be 106.59°F (41.44°C) and 100.07°F (37.82°C), respectively, for the 99°F (37.22°C) ambient used in the present analysis. For the ambient temperature between 56°F (13.33°C) and 85°F (29.44°C), STS flights were generally launched in the morning when the east SRM/RSRM receives more sunlight. Therefore, the east SRM/RSRM surface temperature would be higher than the west SRM/RSRM surface temperature.

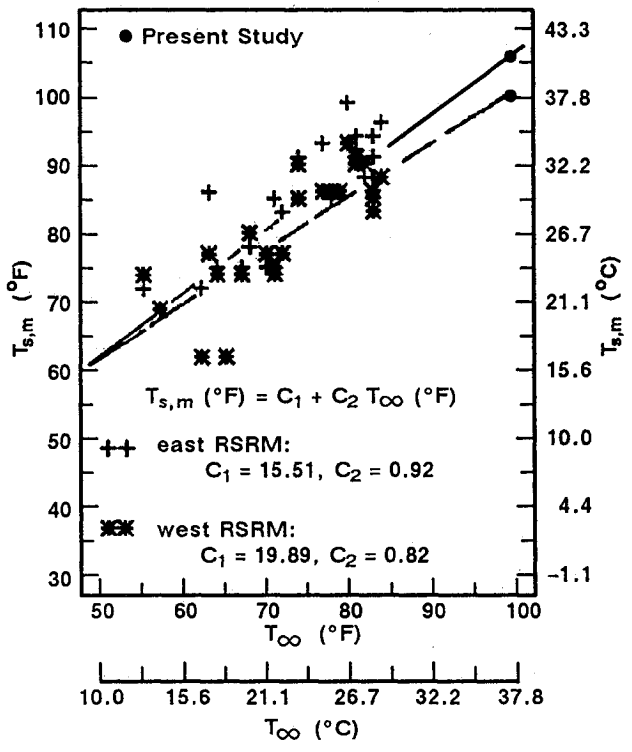

Fig. 9 Peak prelaunch surface temperature measured on east and west RSRMs prior to launch.

2) Local Nusselt number profiles around the RSRMs and ET are shown in Figs. 8a and 8b, respectively. Convective heat transfer results are highly dependent on flow conditions. The approaching flow bifurcates around each component with different degrees of crowding, due to different local flow acceleration. The degree of streamlines crowding on the east RSRM is denser for $150 \leq \theta$ (deg) ≤ 270 than for the west RSRM. Hence, local Nusselt number values are higher on the east RSRM.

Consider the curve showing the local Nusselt number around the west RSRM shown in Fig. 8a. Starting at the forward stagnation point ($\theta = 150$ deg), $Nu_D(\theta)$ decreases with increasing θ due to laminar boundary-layer development, and a minimum ($Nu_D = 1626$) is reached at $\theta \simeq 287$ deg where separation occurs.

Similarly, consider the curve showing the local Nusselt number around ET shown in Fig. 8b. Then, in considering half of the cylinder, starting at the forward stagnation point ($\theta = 150$ deg), $Nu_D(\theta)$ decreases with increasing θ due to laminar boundary-layer development, and a minimum ($Nu_D = 5600$) is reached at $\theta = 228$ deg. At this point, separation occurs and $Nu_D(\theta)$ increases with increasing θ due to acceleration from venturi effects. The maximum Nusselt number obtained by Giedt[32] was achieved by wake mixing, while in the present study it was due to venturi effect. Interestingly, the local Nusselt number profile around the west RSRM (Fig. 8a) looks qualitatively similar to Giedt's results around a single cylinder for $Re_D = 0.708 \times 10^5$. The local Nusselt number profile around the ET looks qualitatively similar to Giedt's results for $Re_D = 2.19 \times 10^5$.

The average Nusselt numbers around the west RSRM, east RSRM, and ET were calculated to be 2205, 3043, and 5714, respectively.

Comparison with Other Studies

There are numerous studies on forced convective heat transfer which apply to single cylinder,[32] multiple cylinders of the same size in tandem,[33] and aligned and staggered tube banks.[33] These studies have been conducted for comparatively small geometries, and not for components of the size used in the STS. Since heat transfer was believed to be dependent upon component size, and since this information was also lacking for large components that are arranged as in the STS, the need for the present study was obvious. Despite these differences, comparing the current results with those in related but different studies is desirable.

The problem of a small, single, cylinder placed normal to a fluid stream has been experimentally investigated by Giedt,[32] where the local Nusselt numbers around the cylinder were determined for $7.08 \times 10^4 \leq Re_D \leq 2.19 \times 10^5$. The size and geometry of the cylinder used in this investigation was markedly different from that in the present study where the geometry was composed of three large cylinders and an orbiter wing (Fig. 4). The SRM/RSRM diameter is 36 times larger than the small, 4-in. (10.16-cm) cylinder used in Giedt's experiment. This means that to achieve equivalent Reynolds numbers in the flow around the SRMs/RSRMs and Giedt's cylinder, the velocity used in this study would have had to have been decreased 36 times, assuming constant viscosity.

Since STS geometry is more complex than a single cylinder, the best comparison was believed to be the local Nusselt number at the forward stagnation point on the west RSRM, since it was in line with the assumed northwest wind direction. In addition, a comparison was made based on the average values of the Nusselt number around the west RSRM. These comparisons are discussed in the following subsections.

Local Nusselt Number at Forward Stagnation Point

In this subsection, three comparisons are made between the local Nusselt number at the forward stagnation point of the west RSRM and that of a single cylinder, a cylinder in an aligned tube arrangement, and a cylinder in the entrance of a staggered tube bank.

Single Cylinder Approach

Schlichting[34] recommended the following expression for calculating the forced convective Nusselt number for incompressible crossflow of air at the forward stagnation point on a cylinder:

$$Nu_{D,\text{fsp}} = (Re_D)^{1/2} \tag{7a}$$

where the exponent of one-half for Re_D indicates the laminar nature at the forward stagnation point. However, experimental results of Giedt[32] show somewhat different behavior when fitted by the present author (using the least-squares method) as

$$Nu_{D,\text{fsp}} = 0.1743(Re_D)^{0.6541}$$

$$\text{for} \quad 0.708 \times 10^5 \leq Re_D \leq 2.19 \times 10^5 \tag{7b}$$

Purely laminar conditions are difficult to achieve experimentally. Effect of freestream turbulence intensity on heat transfer was shown in Ref. 35.

For case 2, with solar heating, the calculated local Nusselt number for the west RSRM at its forward stagnation point ($\theta \simeq 150$ deg) was 2375 (Fig. 8a). The Reynolds number calculated in the present study was 6.78×10^5 and 1.56×10^6, based on the west RSRM and ET diameters, respectively. Using the Reynolds number of 6.78×10^5, based on the west RSRM in Eqs. (7a) and (7b), yields Nusselt number values of 823 and 1136, respectively. Using the Reynolds number of 1.56×10^6, based on the ET in Eqs. (7a) and (7b), yields Nusselt number values of 1248.99 and 1959.84, respectively.

Aligned Tube Bank Arrangement Approach

Following the procedure given in Ref. 32, the maximum Reynolds number is $Re_{D,\max} = U_{\max}(y, z)\, D/\nu$. The maximum velocity $[U_{\max}(y, z)]$ occurs in the spacing [$s = 1$ ft (0.31 m)]

Table 2 Forced convection Nusselt number from cylinders in crossflow

No.	Reference	Equation	C	m	$n1$	Range of Re_D	$\overline{Nu}_D$	$\bar{h}^a$	$\bar{h}^b$
1	Present	——	——	——	——	6.75×10^5	2205	2.83	16.07
2	2	1	——	——	——	——	2182	2.80	15.89
3	32	10	0.027	0.805	0.33	4.0×10^4–4.0×10^5	1186	1.53	8.68
4	32	10	0.076	0.700	0.37	2.0×10^5–1.0×10^6	805	1.04	5.91
5	36	10	0.021	0.814	0	5.0×10^4–2.0×10^5	1168	1.49	8.46
6	36	10	0.328	0.560	0	8.0×10^3–1.0×10^5	603	0.78	4.43
7	36	10	0.270	0.600	0	6.0×10^3–1.3×10^5	849	1.09	6.19
8	36	10	0.157	0.640	0	5.0×10^3–4.2×10^5	845	1.09	6.19
9	36	10	0.500	0.540	0	3.9×10^4–1.1×10^5	703	0.90	5.11
10	36	10	0.143	0.670	0	2.0×10^4–1.2×10^5	1151	1.48	8.40
11	36	10	0.150	0.670	0	3.0×10^4–1.2×10^5	1208	1.55	8.80
12	36	10	0.380	0.560	0	4.0×10^4–1.3×10^5	699	0.90	5.11
13	36	10	0.063	0.720	0	1.3×10^5–3.0×10^5	992	1.28	7.27
14	36	10	0.360	0.580	0	5.7×10^4–1.2×10^5	866	1.11	6.30
15	36	10	0.185	0.620	0	1.0×10^3–2.0×10^5	761	0.98	5.57
16	36	10	0.023	0.800	0	$>5.0 \times 10^4$	1060	1.36	7.72
17	36	10	0.330	0.600	0.33	——	925	1.19	6.76
18	9	——	——	——	——	2.11×10^6	2500	2.93	16.64
19	15	——	——	——	——	1.00×10^5	158[c]	——	——

[a]Btu/h-ft²-°F. [b]W/m²-°C.
[c]Around aft cylinder (corresponds to east RSRM of the present study) in a tandem three-cylinder model (no orbiter wing). Re_D was based on the larger-center cylinder diameter [2.25 in. (5.72 cm)]. Had the Reynolds number calculation been based on the front cylinder [1.0 in. (2.54 cm)], the resulting value would have been 4.55×10^4.

between the RSRM and ET. From the mass conservation requirement for an incompressible fluid

$$U_{max}\,(y, z)\,(s) = (U_\infty \sin 30)[(D_{ET} + D_{RSRM})/2 + s] \quad (8)$$

where D_{ET} and D_{RSRM} are the diameters of the ET and west RSRM, respectively. Substituting the values of U_∞, s, D_{ET}, and D_{RSRM} yields $U_{max}(y, z) = 105$ ft/s (32.00 m/s) and $Re_{D,max} = 7.00 \times 10^6$. Using this value for $Re_{D,max}$ in Eqs. (7a) and (7b) yields Nusselt number values of 2645.34 and 5232.10, which are higher than the value in the present study by 11.38 and 120.30%, respectively.

Staggered Tube Bank Arrangement Approach

Baughn et al.[33] presented experimental data for the local Frossling number $[Fr(\theta)]$ for a single cylinder, cylinders in tandem, and cylinders located in the entrance of an aligned and staggered tube bank. The local Frossling number at the forward stagnation point as a function of Re_D was selected from Figs. 4 and 5 of Ref. 33 for cylinders located in the entrance of a staggered tube bank. Frossling numbers of 0.7, 0.85, 1.0, 1.4, 1.6, and 1.88 respectively correspond to the Reynolds numbers of 27,200, 36,400, 34,700, 34,500, 84,600, and 200,000. This data was best fitted in this study (using the least-squares method) as

$$Fr_{fsp} = Nu_{D,fsp}/(Re_D)^{1/2} = 0.5316\sqrt{(Re_D)} - 4.536 \quad (9)$$

Using the Reynolds number of 6.78×10^5 (based on the west RSRM diameter) in the above equation yields a Nusselt number value at the forward stagnation point of 2142.63, which is smaller than the present value by 9.81%.

Based on these three different methods, the present value for the Nusselt number at the forward stagnation point of the west RSRM is reasonable.

Average Nusselt Number

The average forced convective Nusselt number for a gas flowing normal to a single smooth cylinder can be represented by

$$\overline{Nu}_D = \bar{h}D/k = C(Re_D)^m(Pr)^{n1} \quad (10)$$

where the coefficient, C and exponent, m, are functions of the Reynolds number Re_D, and the exponent $n1$ is a function of Pr, respectively. This equation with different parameters

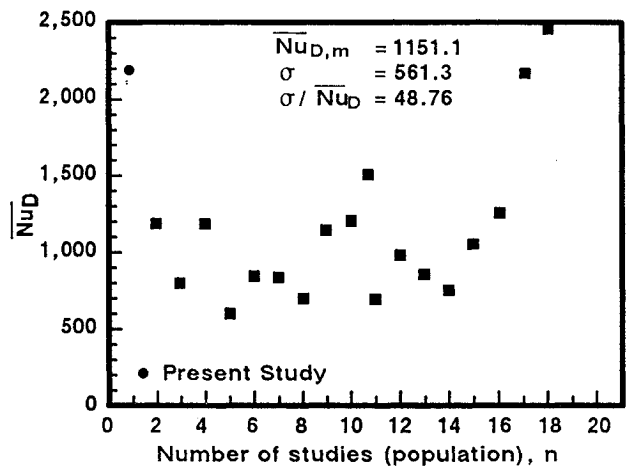

Fig. 10 Forced convection heat transfer from cylinders in crossflow.

is also derived by Hilpert,[32] Zhukauskas,[32] Morgan,[36] and Ahmad and Qureshi[35] (Table 2).

Results from applying the correlations given in Eqs. (1) and (10) to calculate the average values of the Nusselt number are shown in Table 2. The calculated Reynolds number of 6.78×10^5 (based on the west RSRM diameter) was arbitrarily used in each of the correlations so that a direct comparison of the predicted values from Eqs. (1) and (10) could be made with the PHOENICS '81 result.

Figure 10 shows the 18 predicted values of the average Nusselt number for the west RSRM, and for a single cylinder (Table 2), where σ denotes the unbiased or sample standard deviation. The calculated average circumferential value of the west RSRM surface Nusselt number was 2205, which is 91.56% larger than the mean value. Based on a tolerance analysis,[18] it was concluded that, even with increased population size as a result of additional experiments, there is reasonable confidence that the Nusselt number will be less than 3394.

Summary and Conclusions

The present solution provides an accurate flow/thermal description of the STS launch pad environment after the ET has been filled and under the severest summer conditions.

Results are presented as local and average values of the Nusselt number and surface temperature around the RSRMs and ET. Solar heating effects increased the surface temperatures of the RSRMs by 9–11°F (5–6.11°C). Surface tem-

peratures calculated on the west and east RSRMs in this study are in excellent agreement with measured data.

Despite the limitations outlined earlier, comparing the current results with those in previously reported studies is desirable. Since STS geometry is more complex than a single cylinder, the best comparison was believed to be the local Nusselt number at the forward stagnation point on the west RSRM, since it was in line with the assumed northwest wind direction. In addition, a comparison was made based on the average values of the Nusselt number around the west RSRM.

Acknowledgments

This study was supported by the NASA Marshall Space Flight Center under Contract NAS8-30490. The author wishes to thank Stanton Boraas, Ronald Webster, and Robert Regl for reviewing this manuscript.

References

[1]Sutton, G. P., and Ross, D. M., *Rocket Propulsion Elements*, 5th ed., Wiley, New York, 1986, Chap. 10, p. 266.

[2]Anon., "Atmospheric Heat Transfer to Vertical Tanks Filled with Liquid Oxygen," Arthur D. Little, Inc., Special Rept. 50, Cambridge, MA, Nov. 1958.

[3]Maw, J. F.,"STS-51L SRM Grain and O-Ring Temperature Calculations," Action Item 2-18-001, Morton Thiokol, Inc., TWR-30014, Brigham City, UT, Feb. 1986.

[4]Anon., "Thermal Modeling of the Space Shuttle Launch Configuration," SRS Tech., SRS/STD-TR86-022, 604a, Final Rept., Huntsville, AL, March 1986.

[5]Mahaffey, W. A., and Keeton, L. W., "Numerical Analysis of Pre-Launch Thermal Environment of the Space Shuttle, Volume 1: Numerical Model and Results," Concentration Heat and Momentum Limited of North America, TR/4045/53, Huntsville, AL, Sept. 1986.

[6]Singhal, A. K., Tam, L. T., Bachtel, F., and Vaniman, J., "Thermal Environment Around the Space Shuttle with Hot-Gas Jets for Ice Suppression," *Journal of Spacecraft and Rockets*, Vol. 23, No. 6, 1986, pp. 547–553.

[7]Mahaffey, W. A., Smith, C. E., and Singhal, A. K., "Numerical Analysis of Pre-Launch Thermal Environment Around Solid Rocket Booster of Space Shuttle, Volume 1: Numerical Model and Results," Concentration Heat and Momentum Limited of North America, TR/4045/61, Huntsville, AL, Dec. 1986.

[8]Gulrajani, B. K., "Launch Pad Natural Environments for Global Thermal Analysis," Morton Thiokol, Inc., TWR-16604, Brigham City, UT, May 1987.

[9]Mongan, R. D., "Thermal Interfaces Design Data Book (TIDDB) Prelaunch Verification Status Review Meeting, a Presentation," Rockwell International, Downey, CA, Aug. 1987.

[10]Anon., "Documentation of Convective CFD Analytical Support to the TIDDB Verification," Rockwell International, 112-041-B11-01, Huntsville, AL, Oct. 1987.

[11]Ahmad, R. A., and Tran, T. M., "External Flow and Thermal Fields Around the Space Shuttle on the Launch Pad," Morton Thiokol, Inc., TWR-16766, Rev. A, Brigham City, UT, Nov. 1987; see also TWR-16766, June 1987.

[12]Hughes, J. T., and Wilson, M. E., "Space Shuttle Program Thermal Interfaces Design Data Book," Rockwell International, Rept. SD 74-SH-0144E, Downey, CA, Dec. 1987.

[13]Ahmad, R. A., and Boraas, S., "External Tank Chill Effect on the STS Launch Pad Environment," *Journal of Spacecraft and Rockets*, Vol. 28, No. 3, 1991, pp. 306–314.

[14]Ahmad, R. A., Mathias, E. C., and Boraas, S., "Gaseous Oxygen Cooling of the STS Launch Pad Environment," *Journal of Spacecraft and Rockets*, Vol. 28, No. 6, 1991, pp. 689–697.

[15]Miller, L. S., "Basic Aerodynamic and Heat Transfer for Spacecraft Boosters in Pre-Launch Conditions," AIAA 30th Aerospace Sciences Meeting and Exhibit, AIAA Paper 92-0710, Reno, NV, Jan. 1992.

[16]Ahmad, R. A., Mathias, E. C., and Boraas, S., "Negatively Buoyant Flow Along Vertical Cylinders at High Rayleigh Numbers," *Heat Transfer Engineering an International Quarterly*, Vol. 13, No. 2, 1992, pp. 89–103; see also AIAA Paper 90-2723, July 1990.

[17]Mathias, E. C., and Ahmad, R. A., "Thermal Modeling of the Shuttle Solid Rocket Motors on the Launch Pad," *Journal of Spacecraft and Rockets* (to be published); see also AIAA Paper 89-2873, July 1989.

[18]Ahmad, R. A., "The Space Transportation System Summer Environment on Launch Pad," AIAA/SAE/ASME/ASEE 28th Joint Propulsion Conf., AIAA Paper 92-3850, Nashville, TN, July 6–8, 1992.

[19]Gunton, M. C., Rosten, H. I., Spalding, D. B., and Tatchell, D. G., "PHOENICS an Instruction Manual," Concentration Heat and Momentum Limited of North America, TR-75, Huntsville, AL, 1983.

[20]Singhal, A. K., and Owens, S. F., "Introduction to PHOENICS," Concentration Heat and Momentum Limited of North America, Huntsville, AL, Feb. 1984.

[21]Anon., "Systems Improved Numerical Differencing Analyzer, Version SINDA-85," Univ. of Georgia, COSMIC Program MSC-20891, Athens, GA, Feb. 1986.

[22]Jensen, C. L., and Goble, R. G., "Thermal Radiation Analysis System (TRASYS) User's Manual," NASA Johnson Space Center, Houston, TX, Oct. 1986.

[23]Anon., "Thiokol Flight Motor Set Final Report," Thiokol Corp., Repts. TWR-17540-1 through TWR-17544-10 for Flights STS-26 through STS-47, Brigham City, UT, Sept. 1988–Sept. 1992.

[24]Oosthuizen, P. H., and Taralis, D. N., "Combined Convective Heat Transfer from Vertical Cylinders in a Horizontal Fluid Flow," ASME-AIChE Heat Transfer Conf., Paper 76-HT-41, St. Louis, MO, Aug. 1976.

[25]Collis, D. C., and Williams, M. J., "Two-Dimensional Convection from Heated Wires at Low Reynolds Number," *Journal of Fluid Mechanics*, Vol. 6, Pt. 3, Oct. 1959, pp. 357–384.

[26]Patankar, S. V., *Numerical Heat Transfer and Fluid Flow*, McGraw-Hill, New York, 1980.

[27]Launder, B. E., and Spalding, D. B., "The Numerical Computation of Turbulent Flows," *Computer Methods in Applied Mechanics and Engineering*, Vol. 3, North-Holland, Amsterdam, 1974, pp. 269–289.

[28]Ahmad, R. A., and Tran, T. M., "Flow and Thermal Fields Around a Large Single Solid Rocket Motor at High Reynolds Numbers," Morton Thiokol, Inc., TWR-16919, Brigham City, UT, Aug. 1987.

[29]Ahmad, R. A., "Plans Associated with the Flow and Thermal Fields Around the STS," Morton Thiokol, Inc., Interoffice Memo L213-FY87-M089, Brigham City, UT, April 1987.

[30]"Space Shuttle Flight and Ground System Specification, Natural Environment Design Requirements," NASA, National Space Transportation System 07700, Vol. 10, Appendix 10.10, April 1987, pp. 3, 4.

[31]Anon., "Space Shuttle External Tank, Thermal Data Book," Martin Marietta Corp., Michoud Div., Michoud, LA, June 1981.

[32]Incropera, F. P., and Dewitt, D. P., *Introduction to Heat Transfer*, Wiley, New York, 1985, Chap. 7.

[33]Baughn, J. W., Elderkin, M. J., and McKillop, A. A., "Heat Transfer from a Single Cylinder, Cylinders in Tandem, and Cylinders in the Entrance Region of a Tube Bank with a Uniform Heat Flux," *Journal of Heat Transfer*, Vol. 108, No. 2, 1986, pp. 386–391.

[34]Schlichting, H., *Boundary Layer Theory*, 7th ed., McGraw-Hill, New York, 1979, Chap. 12.

[35]Ahmad, R. A., and Qureshi, Z. H., "Buoyancy Effects on Forced Convection from a Uniform Heat Flux Cylinder in a Crossflow," *Journal of Thermophysics and Heat Transfer* (to be published); see also AIAA Paper 92-0711, Jan. 1992.

[36]Morgan, V. T., "The Overall Convective Heat Transfer from Smooth Circular Cylinders," *Advances in Heat Transfer*, Vol. 11, edited by T. F. Irvine and J. P. Hartnett, Academic Press, New York, 1975, pp. 199–264.